Fluorescent Crystallization of Isomeric Quinoline-Capped Thiophene Oligomer in Thin Films Grown by Hot-Wall Epitaxy

Hisao Yanagi,*,†,‡ Kazuhiko Yamane,† Masanori Fukushima,§ and Teruaki Hayakawa|,⊥

Faculty of Engineering, Kobe University, Rokkodai, Nada-ku, Kobe 657-8501, Japan, PRESTO, Japan Science and Technology Agency (JST), 4-1-8 Honcho, Kawaguchi, Saitama 332-0012, Japan, Graduate School of Science and Technology, Kobe University, Rokkodai, Nada-ku, Kobe 657-8501, Japan, and Research Center of Macromolecular Technology, National Institute of Advanced Industrial Science and Technology (AIST), 1-1-1 Higashi, Tsukuba, Ibaraki 305-8565, Japan

Received: July 28, 2003; In Final Form: September 3, 2003

Crystal growth and fluorescent characteristics of a quinoline-capped thiophene oligomer were investigated in thin films grown on the (001) surface of KCl by a hot-wall epitaxy technique. Under controlled substrate and wall temperatures, the deposited film consisted of two types of crystallites: one was epitaxial needles oriented along the $\langle 100\rangle_{KCl}$ and $\langle 110\rangle_{KCl}$ directions, and another was irregular aggregates among them. Fluorescence spectromicroscopy revealed that the former crystals exhibited a red-shifted emission band with respect to the latter. Microscopic Raman spectra for the individual crystallites and vibrational analysis by molecular orbital calculations identified the origin of this fluorescence difference as cis−trans isomerization of the peripheral quinoline groups. In the epitaxial needles, the trans-form molecules were lying parallel to the KCl surface while in the irregular aggregates the cis-form molecules were standing. The detailed crystallization depending on the isomerization was also supported by scanning near-field/confocal scanning laser and transmission electron microscopies.

Introduction

π-Conjugating polymer and oligomer materials have attracted much interest in view of their practical availability to organic optoelectronic devices such as light-emitting diodes (LEDs),[1] field-effect transistors (FETs),[2] and so forth. A variety of molecular design and synthesis methods by changing monomer units and/or conjugation lengths enables us to control their semiconductor properties. Tailoring with various heteroatomic monomer units varies the electronic energy levels of the molecules, which plays an important role in determining their conduction type. Elongated conjugation decreases the band gap between the highest occupied and lowest unoccupied molecular orbitals (HOMO and LUMO), yielding higher conductive species. Furthermore, modification of π-conjugating frameworks and functional groups can convert p-type molecules to n-type ones and vice versa.

Such a control of organic semiconduction is important for future development of molecule-based devices such as p/n junction organic LEDs and laser diodes (LDs). Recent progress of experimental carrier mobilities in organic FETs[3−5] has demonstrated high performances comparable to those of amorphous silicon. We have previously studied light-emitting and FET properties of π-conjugating linear co-oligomers with various sequences and lengths of thiophene and *p*-phenylene units.[6−12] These thiophene/phenylene oligomers are well-sublimed and exhibit stable fluorescence with different colors tuned by their oligomeric structures. Increase of the thiophene units in the *p*-phenylene chain decreases the HOMO−LUMO energy gap, resulting in a red-shift of the fluorescence band. A remarkable feature of these molecules is easy crystallization in regular low-dimensional structures. The co-oligomers recrystallized from a solution formed two-dimensional thin platelets while they epitaxially crystallized in one-dimensional needles with a submillimeter length when grown on the ionic surface of potassium chloride (KCl) by vacuum deposition or hot-wall epitaxy (HWE).[13,14] Under optical excitation, these co-oligomer crystals exhibited amplified light emission, since the fluorescence is confined in the low-dimensional structures and gain-narrowed by their microcavity and self-waveguiding effects. Toward future application of these crysatalline materials to organic LDs, we have been investigating their electrical carrier injection and transport behaviors in FET devices. The recent studies[11,12] have revealed that their hole mobility can be improved up to 0.17 and 0.66 $cm^2\ V^{-1}\ s^{-1}$ by formation of the vapor-deposited platelets and epitaxial needles grown by HWE, respectively. Such high carrier transport can be ascribed to the growth of large domains and favorable molecular orientation in the crystals.

However, all thiophene/phenylene co-oligomers so far investigated only operated in a p-channel accumulation regime. To achieve emissive recombination of injected carriers, it is essential for this class of molecules to be modified having electron transport characters in the crystalline state. From this point of view, in this study we have synthesized a quinoline-capped thiophene oligomer in which the quinoline groups can lower the LUMO level. Although this molecule is well-crystallized in epitaxial needles by the HWE growth, similar to

* To whom correspondence should be addressed. E-mail: yanagi@kobe-u.ac.jp.
† Faculty of Engineering, Kobe University.
‡ PRESTO, Japan Science and Technology Agency (JST).
§ Graduate School of Science and Technology, Kobe University.
| Research Center of Macromolecular Technology, National Institute of Advanced Industrial Science and Technology (AIST).
⊥ Present address: Graduate School of Science and Engineering, Tokyo Institute of Technology, 2-12-1, O-okayama, Meguro-ku, Tokyo 152-8552, Japan.

10.1021/jp036192c CCC: $25.00
Published on Web 10/10/2003

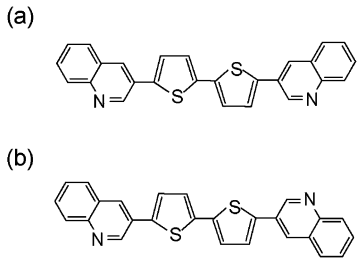

Figure 1. Chemical structures of *cis*-Q2T (a) and *trans*-Q2T (b).

the case of the thiophene/phenylene co-oligomer, a part of the deposited crystals formed irregular aggregates which emitted a fluorescence spectrum different from that of the epitaxial needles. To elucidate the reason for this different fluorescent crystallization, these quinoline-capped thiophene oligomer crystals were examined by means of microscopic fluorescence and Raman spectroscopies, scanning near-field/confocal laser scanning microscopy (SNOM/CLSM) and transmission electron microscopy (TEM).

Experimental Section

Materials. All reagents were purchased from Aldrich, Tokyo Kasei Kogyo Co. (TCI), and Wako Pure Chemical Industries (WAKO) and used without further purification unless otherwise noted. 2,2′-Bithiophene was purified by column chromatography using silica gel with *n*-hexane as the eluent. 2,5-Bis(trimethylstannyl)thiophene was prepared according to a literature procedure.[15]

Synthesis of 2,5-bis(3-quinolyl)thiophene (Q2T) was carried out as follows. In a two-necked round-bottomed flask were placed 2,5-bis(trimethylstannyl)thiophene (0.491 g, 1.0 mmol), 3-bromoquinoline (0.4369 g, 2.1 mmol), and dichlorobis-(triphenylphosphene)palladium(II) (0.007 g, 0.01 mmol). The flask was evacuated and filled with argon three times. Then *N*,*N*-dimethylformamide (20 mL) was added via syringe through a septum rubber cap. The mixture was stirred at 80 °C for 12 h. The mixture was poured into a large amount of methanol. Purification was carried out by recrystallization from chlorobenzene to yield the light orange plate crystals. Yield: 83%. Mp 288.0−289.0 °C. IR (KBr): ν (cm^{-1}) = 1595 (benzene, st), 1565 (C═N, st), 1495, 1420 (thiophene, st), 790, 740 (C−H, st). MS (ESI) *m*/*z* calcd for ($C_{26}H_{16}N_2S_2$: M^+H) 421.0828, found 421.0865. Anal. Calcd for $C_{26}H_{16}N_2S_2$: C, 74.25; H, 3.83; N, 6.66; S, 15.25. Found: C, 74.21; H, 3.75; N, 6.54; S, 15.32.

Optimized structures and molecular properties of Q2T were estimated by molecular mechanics and orbital calculations by the density functional theory (DFT) using an Accelrys Material Studio/DMol^3 program with the DNP basis set and the GGA/BP functional. As assumed from its molecular structure, the rotation of the quinoline groups at both ends gives rise to cis-trans isomers, as shown in Figure 1. Calculation of frontier orbital energies and vibration analysis were performed for *cis*- and *trans*-Q2T.

HWE Growth. Crystal growth of Q2T by the HWE method was carried out using a conventional vacuum evaporator (JEOL JEE-400), as shematically shown in Figure 2. The Q2T sample was loaded in a resistively heated quartz crucible. The (001) surface of a KCl single-crystal fixed on a substrate heater was set 12 cm above the Q2T source. Between the source and substrate, a quartz tube (40 mm i.d.) equipped with a coiled tungsten wire heater was inserted to provide a hot-wall circumstance for evaporated molecules. The substrate temperature (T_s) and wall temperature (T_w) were separately kept at

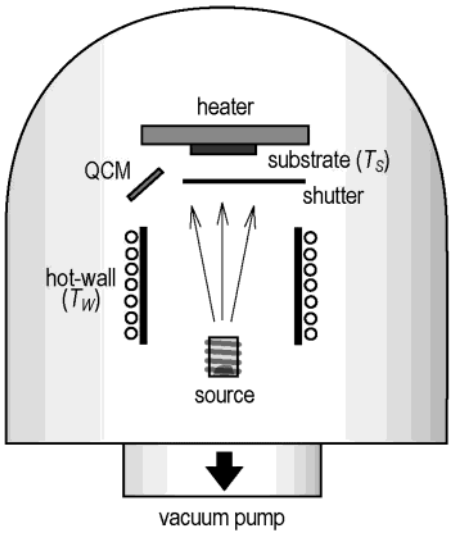

Figure 2. Schematical diagram of the vacuum appararus for HWE.

settled values in the range 120−160 °C under a vacuum of 5×10^{-4} Pa. The deposition rate (R) and thickness were minitored with a quartz crystal microbalance (QCM) set underneath the substrate shutter.

Microscopic Characterization. Fluorescence microscopy and spectroscopy of the deposited Q2T crystals were performed using an inversion fluorescence microscope (Olympus IX-70) equipped with a 250 W high pressure Hg lamp and a CCD multichannel spectrometer (Hamamatsu Photonics PMA-11). A commercially available SNOM/CLSM system (JEOL JSPM-4300) was used for more localized fluorescence characterization. For CLSM measurements, a blue LD excitation beam ($\lambda = 403$ nm) was focused on the scanned sample surface with a 60× objective lens, and the collected fluorescence was introduced to the spectrometer through an optical fiber coupling. In the case of the SNOM mode, a holed Si_3N_4 cantilever set on a 10× objective lens was used as a near-field probe by illuminating the hole with the blue LD. A constant-height scanning was performed with a contact atomic force feedback control with another red LD beam. Microscopic Raman spectroscopy of the deposited crystals was carried out under focused excitation with a 100× objective lens at $\lambda = 647.1$ nm using a 4 mW Ar laser (Spectra-Physics Stabilite 2017-06S). Raman scattering spectra were taken with a double monochromator (Jobin Yvon U1000) and a photomultiplier (Hamamatsu Photonics C-1230). TEM observations were performed at an acceleration voltage of 100 kV using a transmission electron microscope (Hitachi H-7100). For TEM sample preparation, the Q2T crystals reinforced with an amorphous carbon film were transferred onto a copper mesh after dissolving the KCl substrate on the water surface.

Results and Discussion

As compared to a conventional vapor-deposition method where the growth condition is controlled by T_s and R, the HWE technique enables us to perform the crystal growth under optimized conditions close to the thermodynamic equilibrium with another parameter T_w. By using HWE, especially needle-type growth of linear molecules such as *p*-phenylene oligomers has widely been studied.[9,14] The molecules evaporated inside the hot-wall space nucleate at the most stable sites on the substrate surface at a regulated growth rate. The molecules migrating on the surface are then incorporated into the growing edges of the nucleus, resulting in long needlelike crystallites with a length of several hundreds of micrometers. In the present

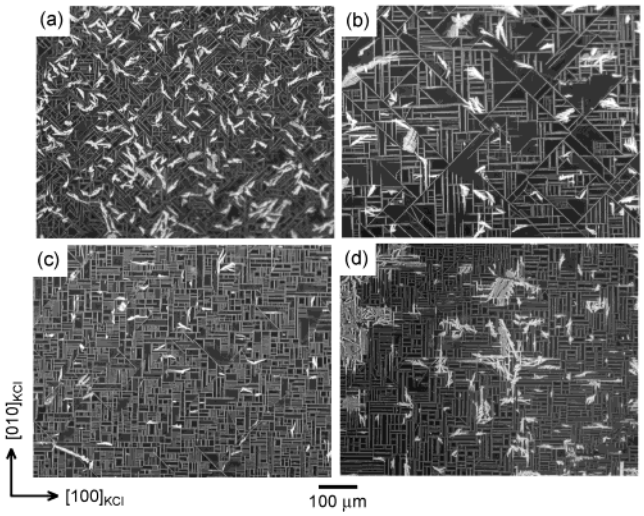

Figure 3. Fluorescence micrographs of Q2T crystals grown on the KCl (100) surface. T_s, T_w, and R are as follows: (a) $T_s = 130$ °C, $T_w = 120$ °C, $R = 1.7$ nm/min; (b) $T_s = 150$ °C, $T_w = 140$ °C, $R = 1.7$ nm/min; (c) $T_s = 130$ °C, $T_w = 120$ °C, $R = 5$ nm/min; (d) $T_s = 160$ °C, $T_w = 150$ °C, $R = 10$ nm/min.

study, we obtained differently oriented crystals of Q2T on the (001) surface of KCl by changing T_s, T_w, and R, as shown in fluorescence micrographs of Figure 3. At $T_s = 130$, $T_w = 120$ °C, and $R = 1.7$ nm/min (Figure 3a), the needlelike crystallites aligning along the ⟨100⟩ and ⟨110⟩ directions of KCl cover the substrate surface. Among these needles, the irregular-shaped aggregates randomly grow, showing brighter fluorescence. With an elevation of T_s and T_w to 150 and 140 °C, respectively, all these crystallites grow larger, keeping their morphology and orientation (Figure 3b). When R is increased to $R = 5$ nm/min, the epitaxial needles orienting along the $\langle 110\rangle_{KCl}$ direction decrease while those along $\langle 100\rangle_{KCl}$ predominantly grow (Figure 3c). This tendency is more prominently seen at $T_s = 160$, $T_w = 150$ °C, and $R = 10$ nm/min (Figure 3d). These observed growth features of Q2T by HWE are considered as follows. An increase of T_s and T_w promotes the migration of evaporated molecules on the substrate surface until they are incorporated at the growing sites of nuclei after long diffusion. This makes the crystal size larger, especially at low R. The disappearance of the needles aligning $\langle 110\rangle_{KCl}$ at higher R suggests that the critical size of this needle nucleus is larger than that of the needles aligning $\langle 100\rangle_{KCl}$. The critical nucleus size becomes smaller as the pressure of the two-dimensional gas composed of the migrating molecules increases in proportion to R. Therefore, the needles along $\langle 100\rangle_{KCl}$ having a smaller critical nucleus size dominantly grow at higher R. Such varied critical nucleation is probably ascribed to the difference in adsorption energy of the Q2T molecule on the ionic lattice of KCl along the ⟨100⟩ and ⟨110⟩ directions, as described later.

As seen in Figure 3, it is noted that the fluorescence intensity and color is different for the epitaxial needles and the irregular aggregates. To identify them, fluorescence spectra were taken from the respective crystallites by excitation through an aperture, as shown in Figure 4. The irregular aggregates (A in Figure 4a) gave an intense fluorescence band with two maximum peaks at $\lambda = 537$ and 570 nm. On the other hand, the spectrum of the epitaxial needles (B in Figure 4a) is weaker and red-shifted, showing a peak at $\lambda = 575$ nm and a shoulder at the longer wavelength side. For this spectral difference, mainly two reasons are supposed: one is crystal polymorphism, and another is cis-trans isomerism of Q2T (Figure 1). To elucidate the former reason, we performed fluorescence spectromicroscopy and

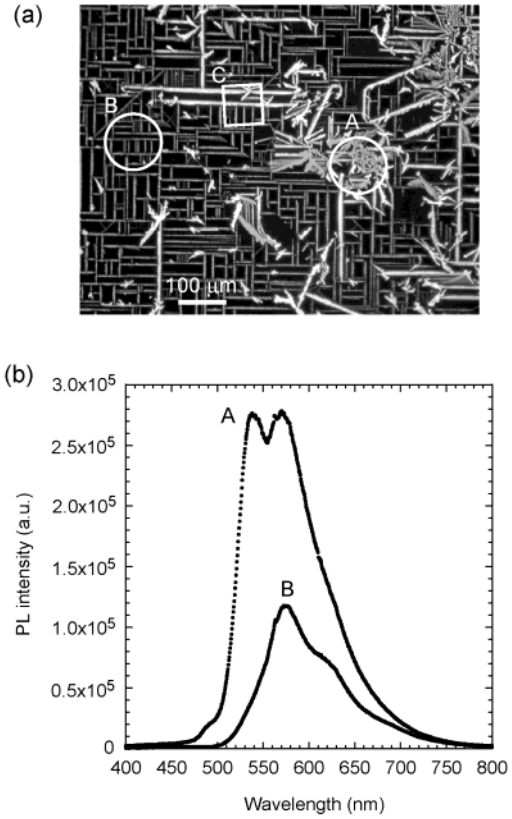

Figure 4. (a) Fluorescence micrograph of Q2T crystals grown on the KCl (100) surface at $T_s = 140$ °C, $T_w = 130$ °C, and $R = 10$ nm/min. (b) Fluorescence spectra taken from the round areas A and B shown in part a.

thermal gravimetry/differential thermal analysis (TG/DTA) for the original powder sample of Q2T recrystallized from a chlorobenzene solution. They revealed two kinds of powdery grains showing different fluorescence bands similar to those shown in Figure 4; however, no prominent signal for the crystalline transition was found.

Therefore, we then examined the existence of cis-trans isomerization in the deposited Q2T crystals by means of microscopic Raman spectroscopy and vibrational analysis by DFT molecular orbital calculations. Parts a and b of Figure 5 show Raman spectra taken from the irregular aggregates and epitaxial needles grown on the KCl surface, respectively. The inset bars on the wavenumber axis indicate the vibration modes calculated for *cis*-Q2T in Figure 5a and *trans*-Q2T in Figure 5b. Since, in both energy-optimized isomer structures, the quinoline and thiophene rings are almost coplanar, the point groups of *cis*- and *trans*-Q2T are assigned to C_s and C_{2h}, respectively. According to their molecular symmetry, in-plane vibrations of *cis*-Q2T, appearing in the wavenumber range 1400−1500 cm^{-1}, are all the Raman-active 'A mode whereas those of *trans*-Q2T are grouped into Raman-active A_g or Raman-inactive B_u modes. The calculated Raman-active vibration modes of 'A for *cis*-Q2T and A_g for *trans*-Q2T well overlap the observed spectra in parts a and b of Figure 5, respectively. Those representative Raman-active vibration modes are schematically shown in Figure 6. Consequently, we conclude that the irregular aggregates are composed of *cis*-Q2T while the epitaxial needles are composed of *trans*-Q2T. This identification by isomeric crystallization is also supported by the frontier orbital energies calculated for *cis*- and *trans*-Q2T. The estimated HOMO/LUMO levels are located at −5.104/−3.101 eV for *cis*-Q2T and −5.058/-3.123 eV for *trans*-Q2T. Therefore, the electronic

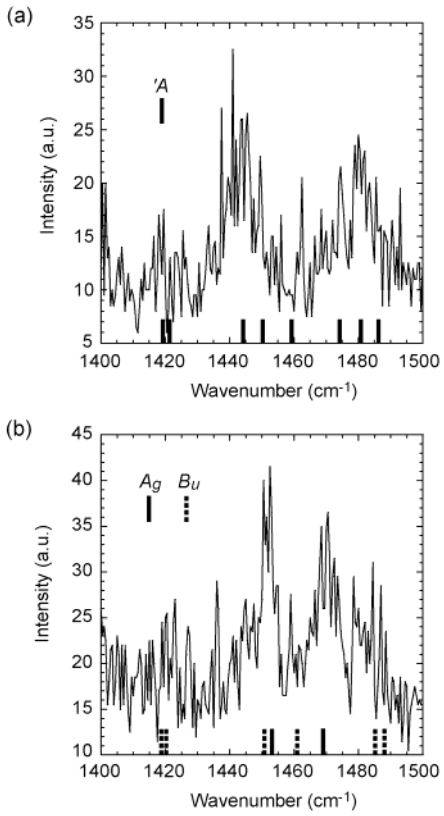

Figure 5. Raman spectromicroscopy taken for irregular aggregate (a) and epitaxial needle (b) crystals. The Raman spectra were assigned to vibration modes calculated for *cis*- (a) and *trans*-Q2T (b), respectively, as shown with bars in the spectra.

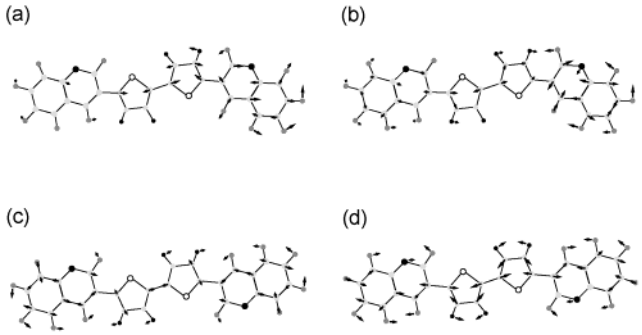

Figure 6. Calculated in-plane vibrations of 'A modes at 1444 (a) and 1481 cm^{-1} (b) for *cis*-Q2T and A_g modes at 1453 (c) and 1469 cm^{-1} (d) for *trans*-Q2T.

transition energies between their HOMO and LUMO orbitals are 2.003 eV for *cis*-Q2T and 1.935 eV for *trans*-Q2T. This energy difference in their HOMO−LUMO transitions well explains the observed spectral shift of the fluorescence bands between the irregular aggregates (*cis*-Q2T) and the epitaxial needles (*trans*-Q2T) (Figure 4).

More detailed isomeric crystallization of *cis*/*trans*-Q2T was examined by spectromicroscopy with CLSM/SNOM and electron diffraction (ED) with TEM. Figure 7a shows a SNOM image taken from the rectangular area as marked as C in Figure 4a. Transmission of the near-field probe light reveals fine structures of the epitaxially grown needle crystals. As can be seen from their different transmission intensities, thinner pleatlike deposits stick to the stem part of the needle. As shown in Figure 7b, fluorescence spectra were separately taken from these individual parts of the crystals by focusing the excitation beams of a blue LD onto the locations marked as D and E in Figure

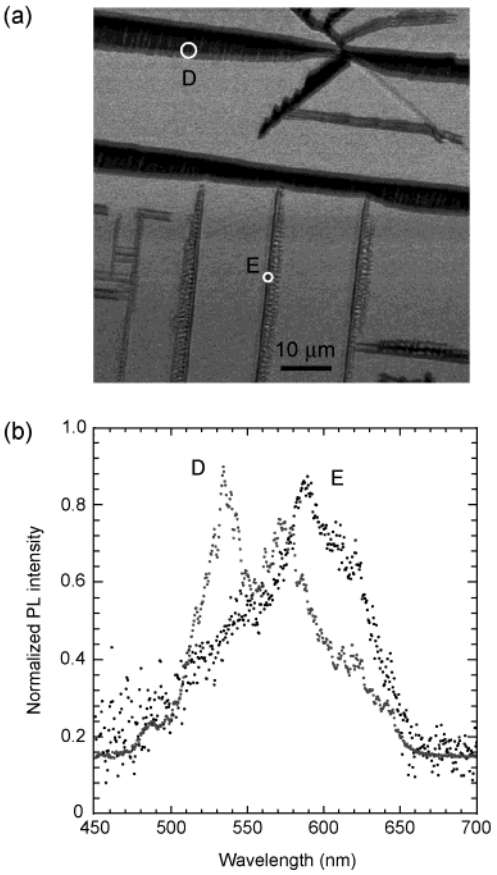

Figure 7. (a) SNOM image of Q2T crystals deposited on the KCl (001) surface. The image was taken from the rectangular area C shown in Figure 4a. (b) Fluorescence spectra taken from the pleatlike part D and the stemlike part E shown in part a. The excitation beam ($\lambda = 403$ nm) was focused on the respective parts using CLSM.

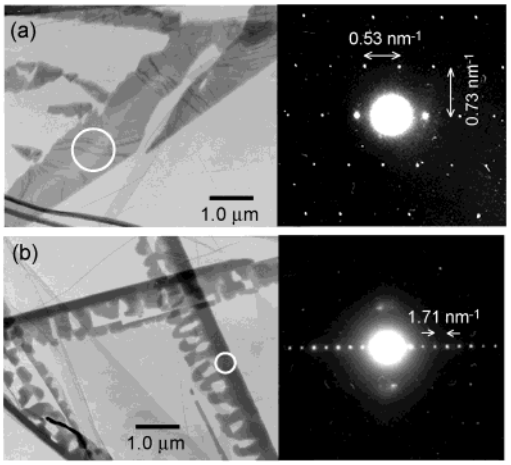

Figure 8. Transmission electron micrographs and electron diffraction patterns taken from the irregular aggregate (a) and epitaxial needle (b) of Q2T.

7a. The pleatlike part D gave a fluorescence band with two peaks at $\lambda = 533$ and 570 nm. This spectrum well resembles that taken from the irregular aggregates (Figure 4A), which is assigned to *cis*-Q2T. On the other hand, the spectrum E in Figure 7b taken from the stem-part of the needle coincides with the red-shifted fluorescence band assigned to *trans*-Q2T (Figure 4B). The locally resolved crystallization of the Q2T isomers was also supported by TEM measurements as shown in Figure 8. The selected-area ED pattern taken from an irregular aggregate indicates reflection spots showing spacings of 0.53 and 0.73

nm (Figure 8a). From an analogy to the ED pattern and crystal structure of thiophene/phenylene co-oligomer crystals,[12,16] these parameters suggest that the molecular axes of the *cis*-Q2T molecules in the irregular aggregates are standing on the KCl (001) surface and are arranged in a herringbone packing. The pleatlike parts sticking to the needle crystal which give an identical ED pattern are clearly seen in the TEM image of Figure 8b. On the other hand, the ED pattern taken from the stem-part of the needle crystal shows a reflection series corresponding to $d = 1.71$ nm (Figure 8b). This long-spacing periodic diffraction suggests that the molecular axis of *trans*-Q2T lies on the KCl surface. However, it is expected that the molecules are slip-stacked by tilting the molecular axis, since the spacing of 1.71 nm is considerably shorter than the molecular length of *trans*-Q2T (~2.3 nm). From the observed two directional orientations of the needles, the *trans*-Q2T molecules epitaxially nucleate along $\langle 100 \rangle_{KCl}$ or $\langle 110 \rangle_{KCl}$. Different interaction forces acting between the molecule and the ionic rows along these two directions probably vary the critical nucleus size of these needle crystals, resulting in dependence of their epitaxial growth on T_s, T_w, and R as is observed in Figure 3.

To conclude, the observed dichromic fluorescence of the deposited crystals is attributed to the cis−trans isomerization of the Q2T molecule. The finding that the pleatlike crystals of *cis*-Q2T nucleate on the needle crystals of *trans*-Q2T also excludes the possibility of polymophism because one crystalline form usually does not nucleate on another form. The different crystalline morphologies and molecular orientations of Q2T depending on the isomerization can be ascribed to the difference in intermolecular interactions of the cis- and trans-forms. The quinoline group in Q2T gives rise to electron localization at its nitrogen position resulting in Coulombic forces between the adjacent molecules. The cis- and trans-configurations of the quinoline groups vary the electrostatic intermolecular interactions in the solid state. Probably, the nitrogen position in *trans*-Q2T prefers the epitaxial nucleation with the ionic surface of KCl while the *cis*-Q2T molecules are more stably arranged in the standing orientation. Although the fluorescence characteristics are also expected to depend on these different crystalline structures, the electronic transition energies attributed to the molecular nature of *cis*- and *trans*-Q2T are dominantly responsible for the observed spectral shift.

Acknowledgment. This work was partly supported by a Grant-in-Aid for Scientific Research (No. 143504980) from the Ministry of Education, Culture, Sports, Science, and Technology. The authors wish to acknowledge Mr. S. Minobe, Faculty of Engineering, Kobe University, and Center for Instrumental Analysis, Kobe University, for Raman spectroscopic measurements.

References and Notes

(1) Burroughes, J. H.; Bradley, D. D. C.; Brown, A. R.; Marks, R. N.; Mackay, K.; Friend, R. H.; Burns, P. L.; Holmes, A. B. *Nature* **1990**, *347*, 539−541.
(2) Fuchigami, H.; Tsumura, T.; Koezuka, H. *Appl. Phys. Lett.* **1993**, *63*, 1372−1374.
(3) Horowitz, G. *Adv. Mater.* **1998**, *10*, 365−377.
(4) Nelson, S. F.; Lin, Y.-Y.; Gundlach, D. J.; Jackson, T. N. *Appl. Phys. Lett.* **1998**, *72*, 1854−1856.
(5) Dimitrakopoulos, C. D.; Malenfant, P. R. L. *Adv. Mater.* **2002**, *14*, 99−117.
(6) Yanagi, H.; Okamoto, H. *Appl. Phys. Lett.* **1997**, *71*, 2563−2565.
(7) Yanagi, H.; Morikawa, T. *Appl. Phys. Lett.* **1999**, *75*, 187−189.
(8) Yanagi, H.; Morikawa, T.; Hotta, S.; Yase, K. *Adv. Mater.* **2001**, *13*, 313−317.
(9) Yanagi, H.; Ohara, T.; Morikawa, T. *Adv. Mater.* **2001**, *13*, 1452−1455.
(10) Nagawa, M.; Hibino, R.; Hotta, S.; Yanagi, H.; Ichikawa, M.; Koyama, T.; Taniguchi, Y. *Appl. Phys. Lett.* **2002**, *80*, 544−546.
(11) Ichikawa, M.; Yanagi, H.; Shimizu, Y.; Hotta, S.; Suganuma, N.; Koyama, T.; Taniguchi, Y. *Adv. Mater.* **2002**, *14*, 1272−1275.
(12) Yanagi, H.; Araki, Y.; Ohara, T.; Hotta, S.; Ichikawa, M.; Taniguchi, Y. *Adv. Funct. Mater.*, in press.
(13) Lopez-Otero, A. *Thin Solid Films* **1978**, *49*, 3−57.
(14) Andreev, A.; Matt, G.; Brabec, C. J.; Sitter, H.; Badt, D.; Seyringer, H.; Sariciftci, N. S. *Adv. Mater.* **2000**, *12*, 629−633.
(15) Seits, D. E.; Lee, S.-H.; Hanson, R. N.; Bottaro, J. *Synth. Commun.* **1983**, *13*, 121−128.
(16) Hotta, S.; Goto, M. *Adv. Mater.* **2002**, *14*, 498−501.